

Ignition enhancement via radical farming in two-dimensional supersonic combustion

J.R. McGuire* R.R. Boyce N.R. Mudford

School of Aerospace, Civil & Mechanical Engineering,
University of New South Wales, Australian Defence Force Academy, Canberra 2600, Australia

Abstract

A two-dimensional numerical study has been performed of the ignition processes associated with the concept of radical farming for supersonic combustion. In a preliminary parametric study, a range of freestream conditions attainable in a hypersonic shock tunnel has been investigated, and mapped according to whether or not the behaviour known as radical farming is present - combustion-induced pressure rise in second or subsequent hot pockets rather than the first. One such case has been analysed in detail, having mean conditions across the combustion chamber entrance that would result in extremely long ignition lengths. The branching cycle and heat release reactions in the combustion process become active in the radical farm, and H and OH radicals are produced. Their rate of production slows in the expansion, but does not approach chemical freezing until towards the end of it. When the mixture flows through the shock at the second hot pocket, the presence of radicals enables the branching cycle and three-body recombination heat release reactions to accelerate, and significant pressure rise due to heat release is then able to occur.

Introduction

There is a particular class of scramjet that is of considerable interest in Australian hypersonics at present: the class in which fuel is injected from the compression ramps in the intake, enabling fuel/air mixing to occur upstream of the combustion chamber. A shock wave in the combustion chamber is then used to elevate the temperature and pressure of the mixture beyond the auto-ignition point. Experimental shock tunnel measurements by Gardner et al [1] in a nominally 2D version of such a scramjet employing discrete porthole hydrogen injection, led to the concept of *radical farming* to describe the chemical kinetic processes that result in ignition and heat release. The flowpath that was investigated by Gardner et al [1] is depicted schematically in Figure 1. In this configuration, and in the absence of fuel injection, hot, high pressure pockets are formed in the flow field between a system of shock and expansion waves propagating along the scramjet. Note that when fuel is injected, the flowfield would become three-dimensional, and if mixing is poor the presence of a layer of cold fuel in the combustion chamber would further modify the flow structure. Figure 2 is an example of the results that pointed to the radical farm concept [11]. It shows the pressure distribution along the combustion chamber lower wall, for injection of hydrogen into both nitrogen and air flows. The former (the lower curve) shows the variation in surface pressure due to a shock/expansion system. The latter (the upper curve) shows the increase in pressure levels that resulted from combustion heat release. In this particular case, the mean conditions across the combustion chamber entrance were insuff-

icient for rapid combustion (approximately 800 K and 80 kPa). On the other hand, the conditions in the first hot high pressure pocket were approximately 1300 K and 200 kPa, sufficient for combustion to occur. The pressure plot of Figure 2 shows that significant release of energy has only occurred once the flow reaches the second region of high temperature and pressure in the combustor.

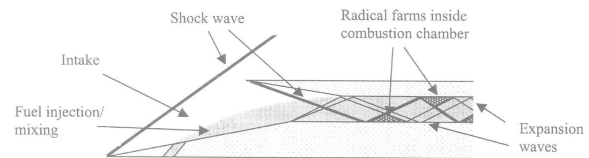


Figure 1: Schematic of scramjet model used by Gardner et al [1]

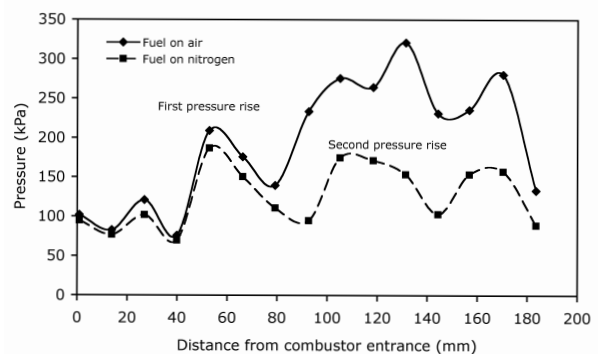


Figure 2: Pressure profiles for reacting and non-reacting flow along the centreline of the model shown in figure 1.

Odam and Paull [10] conducted an experimental investigation of this effect, using fuel injection in a two-dimensional symmetric double ramp intake followed by a straight duct combustion chamber. They demonstrated that in such a configuration, combustion can be achieved even when the mean flow temperature is too low for this to occur without the shock/expansion system that propagates along the combustion chamber. Odam and Paull [10] then postulated the radical farming concept: that in the first region of high temperature and pressure, dubbed the *radical farm*, the flow residence time is long enough to begin production of the chemical radicals such as H and OH that are necessary for ignition and heat release, but not long enough for the latter to occur. Prior to any significant heat release, the supersonic flow passes through an expansion wave in which radical production chemically freezes. Production recommences in hot pockets encountered further downstream, this time with sufficient concentration to allow heat release from combustion

*Systems Engineer, NOVA Defence, Brisbane, Australia

to occur. Depending on the flow conditions, several hot pockets may be necessary to complete this process.

To test this hypothesis, Odam and Paull [10] also conducted a one-dimensional theoretical analysis as follows. A hydrogen-air mixture initially at conditions typical of those in the radical farm was held at the radical farm conditions for a time representative of the residence time in the farm, expanded to typical combustion chamber mean flow conditions over a period representative of the residence time through such an expansion, held at those conditions for a further period of time, and then restored to the original conditions. Their analysis employed a modified form of the reaction scheme of Jachimowski [4]. The results showed that radicals were produced during the residence time in the radical farm, continued production in the expansion until a certain threshold temperature was reached after which their concentration remained approximately constant, and then resumed production accompanied by combustion in the second hot pocket. Their conclusion was that the assumption of frozen radicals in the expansion was reasonable and that the accumulated residence time in the hot pockets was the primary factor that determined the occurrence of combustion.

Radical farming is an extremely significant concept, because it can be used to design scramjets that can operate with milder and hence more efficient intake compressions, such that the mean flow conditions entering the combustion chamber are too cold and/or too low in pressure for auto-ignition to occur. Knowledge of the precise way in which ignition occurs in such scramjets can therefore prove crucial for improving the efficiency and thus viability of scramjet technology. The present paper extends the analysis of Odam and Paull [10], in order to probe the coupling between the combustion kinetics and the flow structures in this class of scramjet. The paper presents a detailed numerical analysis of ignition processes in the radical farm concept of supersonic combustion, using a generic two-dimensional flow-path.

Numerical tools

The numerical tool employed here for the combustion flow-field simulations is the commercial computational fluid dynamics (CFD) code CFD++ [2]. CFD++ can solve both the steady or unsteady compressible and incompressible Navier-Stokes equations, including multi-species and finite-rate chemistry modeling. Thermodynamic modelling of the flow is achieved by applying curve fits to experimental data for each chemical species according to McBride et al [7], while the species transport properties are specified according to the Sutherland law approximation. For turbulent RANS simulations, CFD++ has a range of turbulence models available, from one to three equation transport models. For all calculations in the present work, the two-equation realizable k- ϵ turbulence model was used, with a freestream turbulence level of 2%, and a dimensional turbulence length scale of 0.01m.

The mesh consisted of 80 node points in the vertical direction, and 798 points in the axial direction. In the vertical direction, the node points were clustered towards the wall to assist in resolving the boundary layer flow, however wall functions were also used for this purpose. The distance of the first node point from the wall at the inflow boundary is 0.05mm, while in the

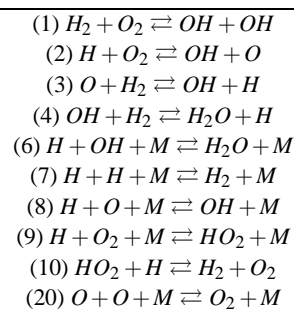
combustor this distance reduces to 0.028mm. In the axial direction, the node points were equally spaced. The wall boundary condition assumed an isothermal wall at 293K, to replicate a shock tunnel flow.

Additional numerical tools were used in order to provide the inflow parameters for the simulations. These simulations have been performed at conditions typically attainable in hypersonic shock tunnel facilities, in order to be relevant to and guide experimental investigations of radical farming processes[8]. The quasi-one-dimensional thermal equilibrium finite-rate chemistry nozzle expansion code STUBE [13] was employed with the reaction scheme of Lordi, Mates and Moselle [6] to simulate the flow through a Mach 6 shock tunnel nozzle and into the test section for a variety of nozzle reservoir total pressure and temperature. The resulting freestream was chemically and frozen partially dissociated. The freestream conditions were then converted to conditions on the scramjet intake ramp using oblique shock theory, employing the software package HAP [3], and then completely mixed with the desired quantity of cold hydrogen fuel. The resulting conditions were then supplied as inflow boundary conditions for the CFD++ calculations reported here.

Hydrogen-air combustion model

Hydrogen-air combustion is a complex system of reactions involving initial reactants intermediate species and final products. A special class of intermediate species known as *free radicals* or *chain carriers* is particularly relevant to combustion reactions. These are formed when a covalent bond is broken, leaving a bonding electron on each of the resulting species. The unpaired electron makes radical species highly reactive. The relevant radicals for the hydrogen/air system are atomic oxygen, O, atomic hydrogen, H, and hydroxyl, OH.

Table 1: Jachimowski [5] finite-rate chemistry model used for combustion calculations. 10 key reactions, of 33, are shown and discussed in the text.



The hydrogen-air chemistry model used for the present study was developed by Jachimowski [5] and is given in Table 1. This model contains 13 species and 33 reactions. The combustion process can be divided into the *ignition process* (consisting of the *initiation reaction* followed by the *branching cycle*), and the *heat release process*. In Table 1, reaction 1 and, initially, reaction 10 in the reverse direction are the initiation reactions for this model, and result in the production of radicals. Reactions 2, 3 and 4 together increase the number of radicals and are known as the branching cycle. These reactions are not as-

sociated with significant heat release, but are vital to the combustion process because it is not until sufficient concentrations of chain carriers are present that heat release reactions accelerate. Reactions such as reaction 9 on the other hand remove radicals from the system, and are called *termination reactions*. For example, reaction 9 replaces the reactive radical H with the relatively non-reactive HO_2 molecule. Reactions 6, 7, 8 and 20 are the three-body reactions responsible for the majority of the combustion heat release. Because they are three-body reactions, they depend on the concentration of radicals being high in order for significant heat release to occur, and thus depend on the branching cycle. They are thus also highly sensitive to pressure, whereas the two-body branching cycle reactions are more sensitive to temperature. In summary, the temperature-sensitive ignition process depends on two-body reactions that produce radicals, while the pressure-sensitive heat release process depends on the ignition process to produce the necessary radicals and then on the three-body reactions that recombine the radicals and produce H_2O . A useful definition of ignition is that it occurs when the concentration of the H radical reaches a maximum (after which the recombination reactions quickly consume it) [9]. The temperature- and pressure-dependent finite-rates at which the various steps in the combustion process occur are critically important in the context of supersonic combustion flowfields.

Mesh Sensitivity Study

A mesh sensitivity study was conducted to check the accuracy of the results obtained for both the parametric study and the subsequent more detailed analysis. A coarser mesh consisting of 60 node points in the vertical direction, and 598 points in the axial direction was examined, along with a finer mesh consisting of 120 points in the vertical direction, and 1198 points in the axial direction. Node points in the axial direction were spaced equally for each mesh, while the same distribution function was used for the points in the vertical direction. The freestream conditions used are given later in Table 2.

In Figure 3, the pressure profiles along the lower surface of the scramjet model for frozen chemistry calculations on each mesh are compared, along with the same profiles for a finite-rate chemistry calculation. The pressure profiles for the frozen chemistry calculation are almost identical, indicating that these solutions are mesh independent. The profiles for the finite-rate calculations however indicate slight differences in the solutions obtained on each mesh. Apart from the first hot pocket, where the peak pressure level in this region depends on the mesh, the remainder of the flow displays an almost identical level of pressure across each shock and expansion wave. The major difference lies in the location of the shock waves in the combustor, where the solution on the standard mesh shows that the shocks are displaced slightly from their corresponding location on the coarse and fine mesh. The overall accuracy of the results is thought to be unaffected by these differences.

Preliminary parametric study

To generate supersonic combustion flows in which radical farming phenomena are present, a preliminary parametric study was performed for the flow through the generic scramjet model, with a premixed H_2 /air mixture entering the model from the left in the figure. The conditions examined cover a range of shock tun-

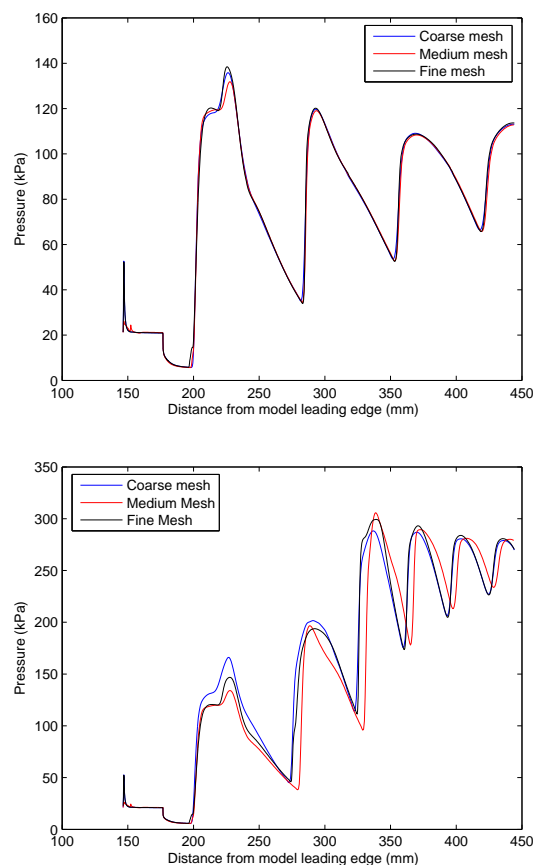


Figure 3: Pressure profiles for the coarse, medium and fine meshes, for non-reacting flow (upper) and reacting flow (lower).

nel nozzle total pressure from 6 to 20 MPa, and a range of total temperature from 2500 to 5000 K. This corresponds to a range of total enthalpy from 2.6 to 7.6 MJ/kg, or flight Mach 7.1 to 12.5. An equivalence ratio, ϕ , of 0.5 was used for all calculations. Pressure contours are shown in the figure for a typical non-reacting solution. A reduced computational domain was used for the calculations in which the main intake ramp begins at the same streamwise location as the cowl. The inflow is set parallel to the intake ramp. The weak shock attached to the ramp leading edge, visible in the figure, results from a leading edge interaction there. Due to the reduced intake length, the boundary layer will not be as developed as it would for a full ramp simulation. This does not alter the key phenomena nor the conclusions resulting from the simulations.

For each test condition, both reacting and non-reacting calculations were performed. Non-reacting flows were realised by specifying frozen chemistry for the simulations. Sample results comparing the reacting and non-reacting pressure profiles along the combustion chamber lower wall are shown in Figure 4, along with a pressure contour plot for each flow. Based on the comparison of pressure profiles, each flow is classified here according to the following definitions:

- Non-combusting: A flow in which the combustion-induced pressure rise is less than 10% at the flow domain

exit,

- **Radical Farming:** A flow in which the combustion-induced pressure rise is less than 10% in the first hot pocket, but greater than 10% at the flow domain exit,
- **Combusting:** A flow in which the combustion-induced pressure rise is greater than 10% in the first hot pocket.

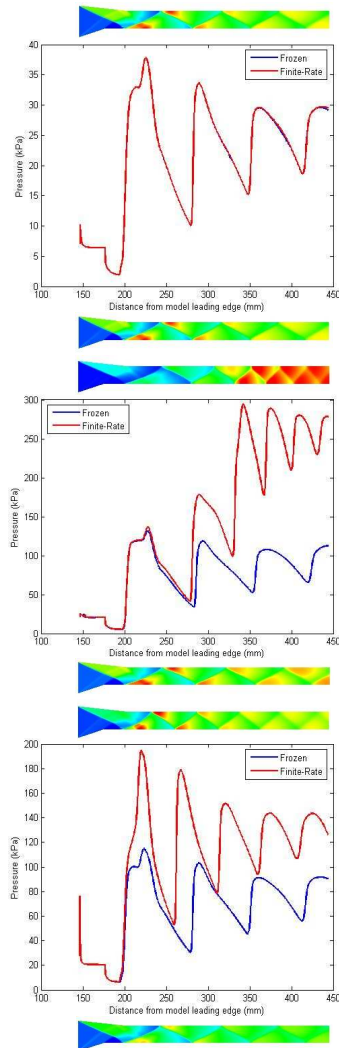


Figure 4: Comparison of pressure profiles for non-combusting, radical farming and combusting flows.

Certain general features in the pressure distributions deserve highlighting. Firstly, the steadily growing mean about which non-combusting pressure oscillates is due to boundary layer growth. Secondly, the amplitude of the oscillations steadily decays, due to the smearing effect of the boundary layer on the shock/expansion system footprint. Thirdly, the double-peak feature on the first hot pocket pressure profile is a result of the weak shock from the intake ramp leading edge reflecting from the cowl and returning to the lower wall. Finally, the transition due to combustion heat release from pre-ignition profiles to post-heat-release profiles can be seen in the figure. For the radical farm case, this occurs approximately over the length of

the second hot pocket, after which the pressure profile behaves as for the frozen case, but at higher levels. This indicates that combustion has been more or less completed by the beginning of the third hot pocket. For the fully combusting case, this has occurred much more rapidly, in the first hot pocket.

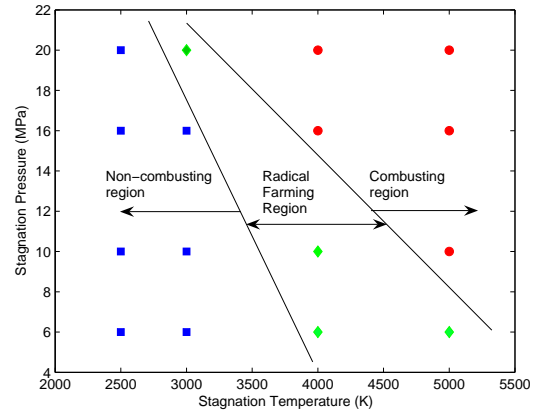


Figure 5: Limits for combustion and radical farming in terms of stagnation temperature and pressure. The squares represent non-combusting flows, the circles represent combusting flows, while the diamonds represent flows that exhibit radical farms.

The results of the classification of the flows as combusting, non-combusting, and radical farming flows, is presented in Figure 5. The radical farming flows appear in a band between non-combusting and combusting flows. The rate of transition between the classifications can be seen from the figure to be more sensitive to changes in total temperature than to changes in total freestream pressure. This can be explained by the greater temperature sensitivity of the initiation reactions, whereas the pressure of the flow has more of an effect on the rate of heat release (in other words, the distance over which the heat release occurs).

Detailed Analysis of Radical Farm Ignition Processes

Table 2 provides the inflow conditions.

Table 2: Inlet conditions for detailed analysis

Pressure (kPa)	20.1
Temperature (K)	400
u-velocity (m/s)	2412
v-velocity (m/s)	382
Global equivalence Ratio (ϕ)	0.5
Mass Fractions:	
H ₂	0.014
O ₂	0.2297
N ₂	0.7559

Using the parametric study above as a guide, a flowfield that would appear to present radical farm ignition behaviour has been generated and analysed in detail. The analysis and comparison is presented below, for the combustion process along a streamline just above the lower wall, and provides insight into

the behaviour of supersonic combustion in this class of scram-jet.

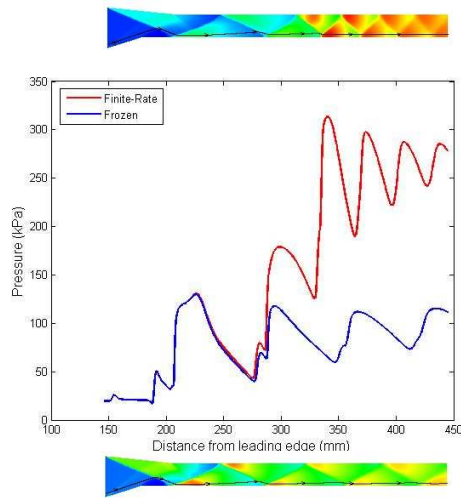


Figure 6: Pressure profiles for combustion and non-combusting flows. Also shown are the pressure contours for the combustion and non-combusting flows above and below the plots respectively.

The pressure profiles for a streamline passing through the radical farm and hot pockets just above the wall for both combustion (reactions switched on) and non-combusting (reactions switched off) flows are shown in Figure 6. These pressure profiles exhibit the radical farming appearance discussed earlier in this paper : rather than combustion-induced pressure rise occurring at the first hot pocket, which begins at approximately 200 mm from the virtual leading edge of the intake ramp, the pressure rise is delayed until the next hot pocket which begins approximately 290 mm from the leading edge. A strong expansion, indicated by a significant decrease in pressure, sits between the first and second hot pockets. The question to be answered here is : are radicals generated in the first hot pocket from initiation and branching cycle reactions, chemically frozen in the subsequent expansion, and then available for the three-body recombination reactions to proceed and release heat in the second hot pocket?

Figure 7 compares the static temperature along the streamlines of Figure 6, for reacting and non-reacting flows. The non-reacting distribution displays strong temperature decreases in the expansion between the first two hot pockets. For the reacting distribution, the temperature decreases in the expansion, but remains slightly higher than the non-reacting version.

Figures 8 and 9 provide information on the production and consumption of the radicals H and OH along the streamline of interest, for both non-reacting and reacting flows. Figure 9 also repeats the pressure distributions, from which the radicals can be correlated with the location of each hot pocket. From the pressure distribution, the first hot pocket begins approximately 205 mm from the leading edge, and the expansion system arrives at approximately 225 mm. The second hot pocket begins at approximately 290 mm. Radicals make their appearance towards the end of the *first* hot pocket, at 220 mm, and *increase* in abun-

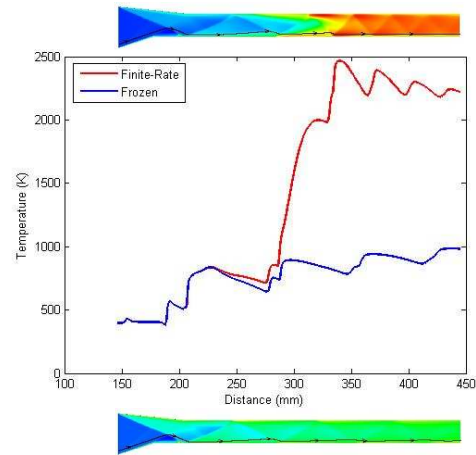


Figure 7: Temperature profiles for combustion and non-combusting flows. Also shown are the temperature contours for the combustion and non-combusting flows above and below the plots respectively.

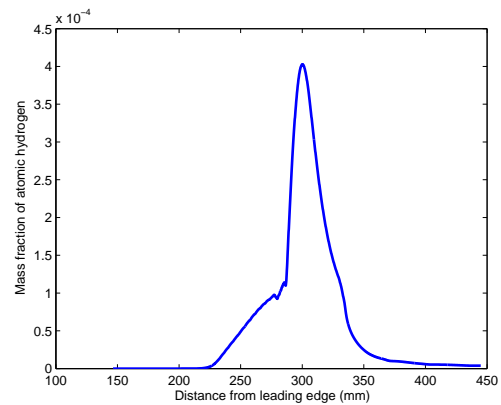


Figure 8: Concentration and mass fraction profiles of atomic hydrogen (H) for the combustion flow.

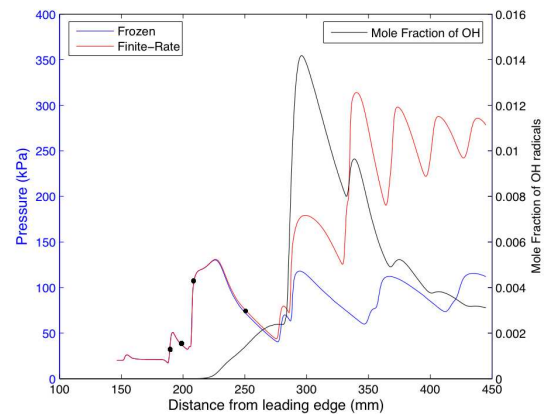


Figure 9: Comparison of finite-rate and frozen pressure profiles, and the profile of mole fraction of OH radicals, along the streamline.

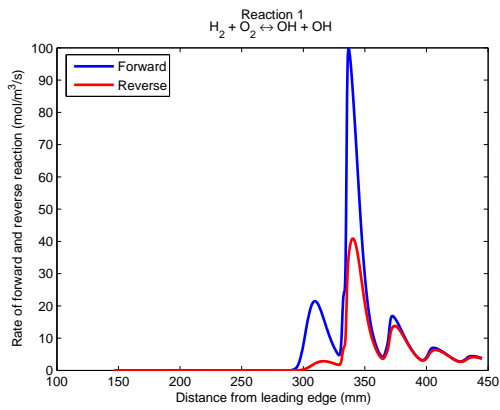


Figure 10: Forward and reverse rates for the initiation reaction 1 along the streamline.

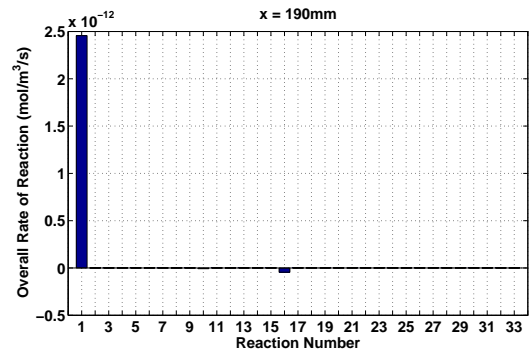


Figure 13: Net reaction rates for each reaction just at the cowl shock, 190 mm.

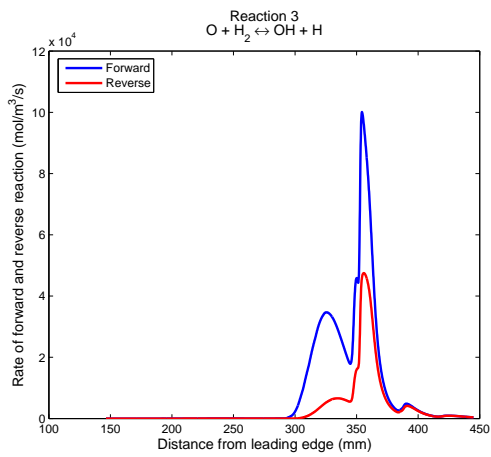


Figure 11: Forward and reverse rates for branching cycle reaction 3 along the streamline.

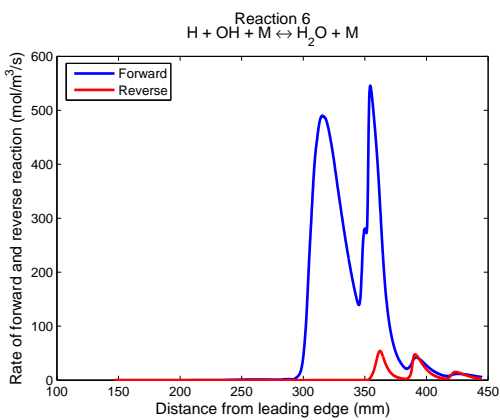


Figure 12: Forward and reverse rates for the highly exothermic 3-body recombination reaction $H + OH + M \rightleftharpoons H_2O + M$ along the streamline.

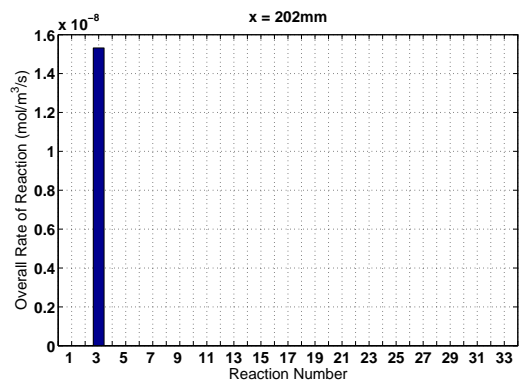


Figure 14: Net reaction rates for each reaction just downstream of the cowl shock, 202 mm.

dance throughout the expansion before plateauing upstream of the second hot pocket, at approximately 270 mm. There is negligible pressure rise due to chemistry over this region, and only a small increment in temperature (Figure 7). This is an indicator that despite the chemical activity that is producing H and OH over this region, the branching cycle and the three-body recombination heat release reactions are not yet significantly active. This is confirmed with the variation of the reaction rates for the initiation reaction R1 (Figure 10), one of the branching cycle reactions R3 (Figure 11), and one of the three-body recombination reactions R6 (Figure 12) - compared to the second hot pocket, reaction rates are very low upstream of the second hot pocket. However, radicals *are* being produced in the first hot pocket. Consider Figures 13 to 16, which show bar charts that provide the net reaction rate for each reaction in the system at the points along the streamline indicated by black dots in Figure 9. At 190 mm, just at the edge of the cowl shock but upstream of the first hot pocket, the initiation reaction R1 is dominant, at *very* low rates. This is enough to enable the branching cycle to become active, and reaction R3 dominates the system behind the cowl shock at 202 mm, again at very low rates. Just inside the first hot pocket at 210 mm, the branching cycle reactions continue to dominate and are now 8 orders of magnitude faster than upstream of the first hot pocket. These reactions continue to accelerate through that hot pocket and into the expansion, such that inside the expansion at 251 mm, they are a further 3 orders of magnitude faster. The reaction rates achieved are sufficient for radical levels to have become appreciable, despite the rates still being insignificant compared with the second hot pocket. In summary, the first hot pocket has initiated the combustion process, radical production has begun, has *not* been quenched by the expansion, but has not occurred at a sufficient rate for ignition to be achieved by the first hot pocket alone. The first hot pocket is indeed a *radical farm*.

As soon as fluid enters the second hot pocket, the rates of the branching cycle reactions rapidly increase (Figure 11) with the forward rates significantly higher than the reverse rates. Radical production accelerates (Figures 8 and 9) such that the recombination heat release reactions also become very active (Figure 12). Heat release raises the static temperature of the flow - the mixture is now reactive. Over the passage through the second hot pocket, the recombination reactions begin to consume the radicals. The levels of H and OH have peaked in the second hot pocket, indicating that ignition has been achieved. The heat release begins the process of increasing the pressure of the system (Figure 9). However, the figures show that the radical consumption and heat release are not completed within the second hot pocket. The expansion after that hot pocket decreases the net rates of the branching cycle and heat release reactions, but not to zero - in other words, chemical activity still proceeds throughout that expansion, radicals continue to be consumed, and heat release continues to raise the temperature. When the fluid reaches the third hot pocket at approximately 340 mm, the branching cycle accelerates once again and produces more radicals - this is most noticeable for OH - which the recombination reactions quickly begin consuming. The temperature now rises to its equilibrium level of approximately 2300 K, and the pressure rises to approximately 250 kPa, about which it oscillates throughout the remainder of the flow. The figures indicate that

some chemical activity also occurs within the fourth and even fifth hot pockets, located at 380 mm and 410 mm respectively, but this activity is very minor in comparison with the second and third hot pockets.

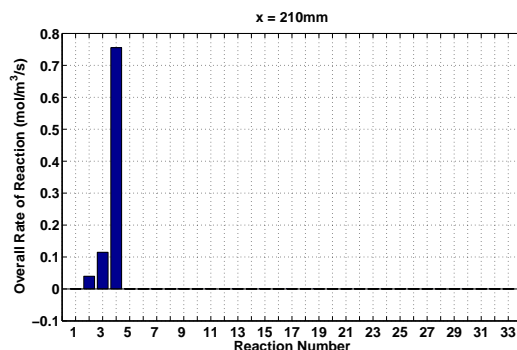


Figure 15: Net reaction rates for each reaction just at the edge of the first hot pocket, 210 mm.

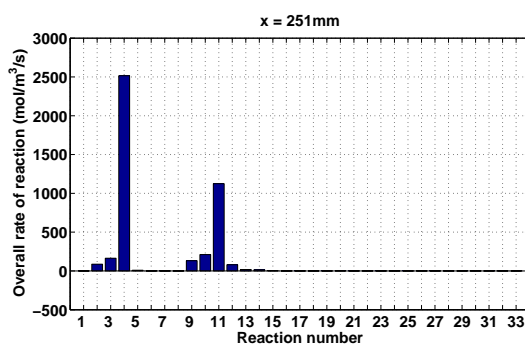


Figure 16: Net reaction rates for each reaction downstream of the first hot pocket, 251 mm.

The combustion presented here is shock-induced combustion, in which shock waves are deliberately used to ignite the flow - in other words, to raise the temperature and pressure to levels where ignition and heat release will occur rapidly. Herein lies a key advantage of radical farming. The temperature and pressure in the radical farm are approximately 800 K and 120 kPa respectively (Figures 6 and 7). These conditions are, as discussed above, non-reactive. The ignition delay time correlation of Pergament [12], developed for standard atmosphere pressure stoichiometric hydrogen-air mixtures, is given by

$$\tau_{id} = 8 \times 10^{-3} \exp(9600/T) \quad \mu s.$$

At the approximate combustion chamber entrance velocities of the work presented here - 2400 m/s - and noting that these velocities do not vary significantly throughout the combustion chamber because they represent the bulk of the energy of the flow, the distance required for ignition would be of the order of 5 m. In the absence of the chemical reactions that have been observed here to occur in the radical farm, the conditions in the second hot pocket would represent no improvement on this situation. However, the reactions have not only generated radicals, but have also raised the temperature of the flow. Inspection of

the reacting and non-reacting temperature profiles at the start of the second hot pocket (Figure 7) indicate that the post-shock temperature in the second hot pocket is approximately 1200 K as a result of the radical farm. At this higher temperature, the distance required for ignition is now of the order of 100 mm according to the correlation above. This is of similar order to the ignition delay length observed in the present work.

Conclusion

A two-dimensional numerical study has been performed of the ignition processes associated with the concept of radical farming for supersonic combustion. In a preliminary parametric study, a range of freestream conditions attainable in a hypersonic shock tunnel has been investigated, and mapped according to whether or not the behaviour known as radical farming is present - combustion-induced pressure rise in second or subsequent hot pockets rather than the first. One case has been analysed in detail, having mean conditions across the combustion chamber entrance that would result in extremely long ignition lengths.

In this case, radicals were produced in and downstream of the first hot pocket via the combustion initiation reaction. This chemical activity slowed in the expansion between the first and second hot pockets, but did not freeze. At the same time, low levels of heat release raised the temperature of the flow. When the mixture reached the second hot pocket, the existence of radicals in the flow and the elevated temperature enabled the branching cycle and recombination heat release reactions to become active. Heat release accompanied by pressure rise occurred throughout the second hot pocket and into the next expansion. This was repeated to a lesser degree in the third and fourth hot pockets. The expected equilibrium pressure level was partly reached in the second and almost fully reached in the third hot pocket.

In summary, for this premixed two-dimensional configuration the first hot pocket does indeed act as a radical farm. The branching cycle and heat release reactions become active in the radical farm, and H and OH radicals are produced. Their rate of production slows in the expansion, but does not approach chemical freezing until towards the end of it. When the mixture flows through the shock at the second hot pocket, the presence of radicals enables the branching cycle and three-body recombination heat release reactions to accelerate, and significant pressure rise due to heat release is then able to occur. The extent to which this is completed in the second hot pocket depends on the inflow conditions.

References

- [1] Gardner A.D., Paull A., McIntyre T.J., *Upstream port-hole injection in a 2D scramjet model*, Shock Waves, Vol. 11, No. 5, pp. 369-375, 2002
- [2] Goldberg U., Peroovian O., Chakravarthy S., Sekar B., *Validation of CFD++ Code Capability for Supersonic Combuster Flowfields*. AIAA Paper No. 97-3271, 1997
- [3] Heiser W.H., Pratt D.T., *Hypersonic Airbreathing Propulsion*, AIAA Education Series (ed. Przemieniecki J.S.), AIAA, 1994

- [4] Jachimowski C.J., *An Analysis of Combustion Studies in Shock Expansion Tunnels and Reflected Shock Tunnels*, NASA TP-3224, 1992
- [5] Jachimowski C.J., *An Analytical Study of the Hydrogen-Air Reaction Mechanism with Application to Scramjet Combustion*, NASA TP-2791, 1988
- [6] Lordi J.A., Mates R.E., Moselle J.R., *Computer Program for the Numerical Solution of Nonequilibrium Expansions of Reacting Gas Mixtures*, NASA CR-472, 1965
- [7] McBride B.J., Gordon S., Reno M.A., *Coefficients for Calculating Thermodynamic and Transport Properties of Individual Species*, NASA TM-4513, 1993
- [8] McGuire J.R., Boyce R.R., Mudford N.R., *Comparison of Computational and Experimental Studies on Shock Induced Ignition in Scramjets* AIAA-2005-3394, 2005
- [9] Nicholls J.A., *Stabilization of Gaseous Detonation Waves with Emphasis on the Ignition Delay Zone*, PhD dissertation, University of Michigan, 1960
- [10] Odam J., Paull A., *Radical Farming in Scramjets*, Notes on Numerical Fluid Mechanics and Multidisciplinary Design, Vol. 96 (eds. Tropea C., Jakirlic S., Heinemann H.-J., Hnlinger H.), Springer, Berlin, 2007
- [11] Paull A., unpublished data, The University of Queensland, 2000
- [12] Pergament H.S., *A Theoretical Analysis of Non-Equilibrium Hydrogen-Air Reactions in Flow Systems*, Proc. AIAA - ASME Hypersonic Ramjet Conference, 1963
- [13] Vardavas, I.M., *Modelling Reactive Gas Flows within Shock Tunnels*. Aust. J. Phys., 37, 157-177, 1984